Applied Catalysis B: Environmental 105 (2011) 306–316

Contents lists available at ScienceDirect

Applied Catalysis B: Environmental

journal homepage: www.elsevier.com/locate/apcatb

Role of metal components in Pd–Cu bimetallic catalysts supported on CeO_2 for the oxygen-enhanced water gas shift

Junichiro Kugai[a], Jeffrey T. Miller[b], Neng Guo[b], Chunshan Song[a,*]

[a] Clean Fuels and Catalysis Program, EMS Energy Institute, and Department of Energy and Mineral Engineering, The Pennsylvania State University, 209 Academic Projects Building, University Park, PA 16802, USA
[b] Chemical Technology Division, Argonne National Laboratory, 9700 South Cass Avenue, Argonne, IL 60430-4837, USA

ARTICLE INFO

Article history:
Received 7 August 2010
Received in revised form 5 April 2011
Accepted 12 April 2011
Available online 20 April 2011

Keywords:
Oxygen-enhanced water gas shift (OWGS)
Water gas shift (WGS)
Pd
Cu
Metal catalyst
CeO_2-supported Pd–Cu
Bimetallic catalysts

ABSTRACT

Catalytic hydrogen production and CO removal in a post-reforming process are critical for low-temperature fuel cell applications. The present study aims at clarifying the role of metal components in bimetallic catalysts for oxygen-enhanced water gas shift (OWGS), wherein a small amount of O_2 is added to H_2-rich reformate gas to enhance CO shift. Among CeO_2-supported bimetallic catalysts, Pd–Cu and Pt–Cu combinations were found to show strong synergetic promoting effect in OWGS, which leads to much higher CO conversion and higher H_2 yield than WGS at low temperature around 250 °C. Temperature programmed reduction (TPR) showed strong interaction between Pd and Cu in Pd–Cu/CeO_2 by a single reduction peak in contrast to multiple peaks on monometallic Cu/CeO_2. Extended X-ray absorption fine structure (EXAFS) analysis revealed that such bimetallic Pd–Cu and Pt–Cu form alloy nanoparticles, where noble metal is mainly surrounded by Cu atoms. Oxygen storage capacity (OSC) measurements point to higher resistance of Pd–Cu to oxidation indicating that Pd keeps Cu in reduced state in air pulse condition. From kinetic study, Pd in Pd–Cu was found to promote CO shift, rather than CO oxidation by increasing the number of active sites and by suppressing H_2 activation (that is inherent to monometallic Pd), which minimizes both the inhibition effect of H_2 and the loss of H_2 by oxidation in OWGS. Transient response technique revealed that Cu in Pd–Cu enhances desorption of strongly chemisorbed CO_2 on catalyst surface in contrast to very slow CO_2 desorption from surface of monometallic Pd. Thus, the excellent OWGS activity of Pd–Cu catalyst has been attributed to the complementary roles of the two metals for enhancing CO shift, which is realized by its alloy structure and the accompanying strong interaction between metal components.

1. Introduction

Hydrogen (H_2) is considered to be a promising clean energy carrier for use in fuel cells which are intrinsically more energy-efficient for power generation compared to internal combustion systems [1–5]. Catalytic reforming of gaseous and liquid hydrocarbons, biomass-derived liquids, and alcohols is an attractive method for H_2 production, especially for fuel cell applications in view of easy handling and safety. One of the drawbacks in this catalytic reforming is the co-production of carbon monoxide (CO) in the H_2 stream. As low as 30 ppm of CO concentration in the H_2 stream severely poisons anode catalysts of proton-exchange membrane fuel cells [6,7]. Therefore, CO must be removed in the downstream, usually by water gas shift (WGS) and further by preferential oxidation (PROX). Conventional catalysts, Fe–Cr for high temperature shift (HTS) and Cu–Zn–Al for low temperature shift (LTS), have been employed for the WGS in stationary hydrogen plants, but these catalysts are not suitable for fuel cell applications due to (i) their slow kinetics and thus large catalyst volume occupying more than 50% fuel processor system volume and (ii) their pyrophoric nature that requires careful pre-conditioning and/or periodical regeneration [1,5,8].

In order to improve the slow kinetics of WGS at low temperatures, our group has been exploring the oxygen-enhanced water gas shift (OWGS) reaction over ceria-supported Pd–Cu bimetallic catalysts, where addition of a small amount of oxygen into WGS feed largely enhanced CO removal from the H_2-rich gas stream at relatively low temperatures [9–11]. It was experimentally proven that CO conversion is higher for OWGS than WGS or PROX on this catalyst system [9]. Sekizawa et al. also reported that addition of O_2 to WGS of methanol reformate gas over Cu/Al_2O_3–ZnO enhanced removal of CO through CO oxidation [12]. It was proposed

* Corresponding author. Tel.: +1 814 863 4466; fax: +1 814 865 3573.
E-mail address: csong@psu.edu (C. Song).

0926-3373/$ – see front matter © 2011 Published by Elsevier B.V.
doi:10.1016/j.apcatb.2011.04.020

that added O_2 facilitates chemisorption of H_2O to form hydroxyl groups, which is believed to be critical in associative and regenerative mechanisms of WGS over Cu catalysts [13,14], and the heat from exothermic surface reaction activates the reaction sites as well [15,16]. However, O_2 addition to the gas containing water at low temperature resulted in deactivation of Cu. The reaction pathway and the effect of O_2 addition to WGS would also be different on ceria-supported catalysts from alumina-supported Cu catalysts and therefore needs to be clarified.

The ceria-supported Pd–Cu catalysts described in our previous report are considered to be low-pyrophoric and therefore suitable for fuel cell applications. The low-pyrophoric nature originates from the unique redox property of metal-loaded ceria, i.e. ease of reduction at low temperature and high redox capacity [17,18], that leads to low Cu loading required for high activity. During OWGS or WGS reaction, ceria is proposed to participate in the reaction through its redox process, keeping metal oxidation state constant as well as providing oxygen to oxidize CO [19–23]. Metal components also have significant impacts on catalytic performance and pyrophoricity as well. For example, Hilaire et al. compared ceria-supported Pd, Ni, Co, Fe and showed that Pd and Ni have higher WGS activity than Co and Fe [24]. Ceria-supported Pd was shown to be promoted by adding iron as an additive, which was conceived to enhance oxygen transport from ceria to CO chemisorbed on Pd sites [17]. Ceria-supported Pt has been reported to be modified by Re to enhance both WGS activity and stability [25]. The Pd–Cu bimetallic catalysts supported on CeO_2 also exhibit better performance than monometallic Cu or Pd catalysts [9]. By the study on surface and structural properties of Pd–Cu bimetallic system on CeO_2 support, it was found that Pd and Cu form alloy with highly dispersed Pd in Cu which could keep Cu in reduced state, being favorable for WGS and OWGS [11]. However, correlation of structural and chemical properties and OWGS activity with bimetallic composition remains to be clarified and the active sites and role of each metal in Pd–Cu catalysts are yet to be identified.

In this context, the first objective of this study is (i) to identify promising bimetallic catalysts supported on CeO_2 for OWGS from various formulations. The metal loadings of Pd–Cu/CeO_2 system were further optimized for a practical OWGS condition wherein high CO concentration and low O_2 (O_2/CO = 0.14) exist in the feed as well as low Cu loading was sought for lower pyrophoricity. The second objective is (ii) to identify the roles of Pd and Cu in Pd–Cu/CeO_2 for OWGS. For this purpose, reducibility (measured by TPR), oxygen storage capacity (OSC), and local structure (measured by EXAFS) for catalysts with various Pd and Cu loadings were investigated and correlated with kinetic data. The impacts of the presence of H_2 and CO_2 in the feed gas on the rates were also investigated for this purpose.

2. Experimental

The catalysts were prepared by wetness impregnation using aqueous solution of tetra-ammine Pt (IV) hydroxide, Rh (III) nitrate, Ir (III) chloride, Cu (II) nitrate, Co (III) nitrate, Fe (III) nitrate, Mn (II) acetate, acetone solution of Pd (II) acetate on cerium oxide. Co-impregnation was carried out for preparing bimetallic catalysts except Pt–Cu/CeO_2. Sequential impregnation was carried out for preparing bimetallic Pt–Cu (copper first, then platinum) and trimetallic catalysts (Pd–Cu first, then Pt or Ir) because these salts did not dissolve with each other in the solution. A commercial ceria (HSA, Rhodia) with 155 m^2/g of specific surface area was used as the support. The metal loadings were 1 wt% for noble metals and 5 wt% for base metals unless specified otherwise. All the catalysts were calcinated at 450 °C for 5 h.

The catalytic activity was tested in a quartz fixed-bed down-flow reactor with 4 mm of inner diameter. The catalyst was pelletized and sieved into 0.25–0.50 mm in diameter, and about 0.1 g of the catalyst was packed into the reactor. The aspect ratio was approximately 1.5. The feed gas which modeled a real reformate had a composition of 9.7% CO/22.8% H_2O/6.3% CO_2/37.9% H_2/6.9% air/argon balance. The H_2O/CO ratio was 2.35 and O_2/CO ratio was 0.14. The space velocity was around 64,400 h^{-1} (dry, excluding air and argon). In the case of WGS, air in the feed was replaced by N_2. Prior to the catalytic reaction, the catalyst was reduced in situ in 7.5% H_2/N_2 flow at 260 °C for 1 h. The effluent of the reactor was analyzed using gas chromatograph (Agilent Micro GC 3000A) equipped with dual channels, one with Molecular Sieve 5A and the other with Plot Q, and TCD detectors. For kinetic study, the gas composition of 9.8% CO/23.0% H_2O/6.9% air/N_2 balance was employed and N_2 concentration was adjusted upon a change of gas composition if necessary, so that total flow rate was always constant. The amount of the catalyst used was 0.015 g. It was diluted by SiC particles of the same size to attain 0.065 ml of the catalyst bed volume.

For the WGS reaction with the O_2 pretreatment, the temperature of the catalyst bed comprised of 0.1 g of 1 wt% Pd–5 wt% Cu on CeO_2 was increased in air up to 260 °C, flushed with N_2, and then WGS feed (9.8%CO/23.0% H_2O/N_2 balance) was introduced. The following O_2 and H_2 pretreatments were conducted (before switching to WGS feed gas) in (1) pure air for an hour, (2) 50% H_2/N_2 for an hour, (3) 10% H_2/N_2 for about 12 h, and (4) 6.9% air/22.8% H_2O/N_2 for an hour, respectively.

The temperature-programmed reduction (TPR) experiments were conducted on Micromeritics Autochem 2910 TPD/TPR equipped with a TCD detector using 50 ml/min of 5% H_2/argon flow with the heating rate of 5 °C/min. Oxygen storage capacity (OSC) was measured using the same equipment by pulsing air at 260 °C after the sample was reduced at the same temperature. Ametek Dycor Dymaxion mass spectrometer DM200 M was employed with Autochem 2910 for detection of oxygen pulses.

X-ray absorption measurements were conducted on the insertion-device beam line of the Materials Research Collaborative Access Team (MRCAT) at the Advanced Photon Source, Argonne National Laboratory. The detailed method is described elsewhere [11]. A short description is given here. The measurements were conducted in situ with reduction atmosphere in transmission mode using a continuous-flow EXAFS reactor cell (18 in. long, 0.75 in. diam.). The catalysts were reduced in 4% H_2/He at 250 °C for 30 min followed by purging with He at 250 °C for 30 min to desorb chemisorbed hydrogen and decompose Pd–H. Then the Pd K edge (24.350 keV) or Cu K edge (8.979 keV) spectra were obtained. Spectra of Pd foil and Cu foil were acquired simultaneously with those of Pd–Cu/CeO_2 samples for energy calibration. Experimental phase and amplitude functions were prepared from Pd and Cu foil. Theoretical phase and amplitude functions for Pt–Cu, Cu–Pt, Pd–Cu and Cu–Pd were prepared using FEFF 8 and calibrated to Pt, Pd and Cu foils to determine the appropriate S_o, the Debye–Waller factor and off-set in *R*.

3. Results and discussion

3.1. Effect of bimetallic catalysts

Fig. 1 shows the CO conversion over CeO_2-supported monometallic catalysts. The metal loadings were 1 wt% for noble metals and 5 wt% for base metals. Fig. 1a presents the measured CO conversion over the catalysts, while Fig. 1b divides CO conversion in OWGS into two parts including the contribution of both CO shift (WGS), and CO oxidation calculated from added

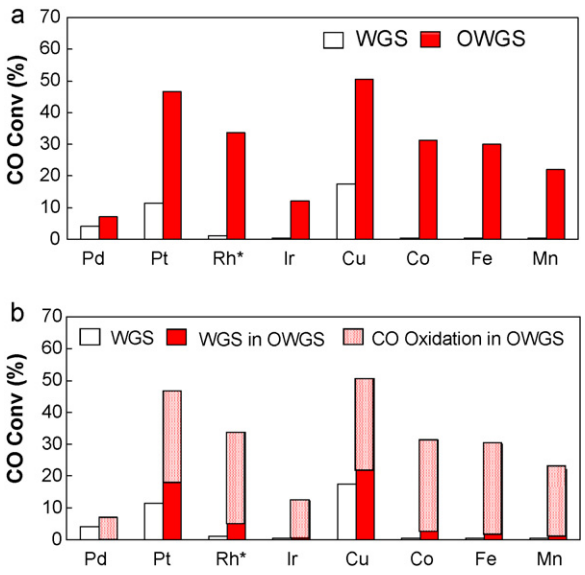

Fig. 1. (a) Screening test results for single metal catalysts supported on CeO_2. Feed: 9.7% CO/22.8% H_2O/6.3% CO_2/37.9% H_2/6.9% N_2 or Air/argon balance, Temp = 260 °C, GHSV = 64,400 h^{-1}(dry); Pd, Pt, Rh, Ir: 1 wt%; Cu, Co, Fe, Mn: 5 wt%. *OWGS on Rh: 30% of CO committed to CH_4 formation reaction. ($2CO + 2H_2 = CH_4 + CO_2$). (b) The CO conversion for OWGS in (a) was divided into contributions of CO oxidation (28.9% of CO conv., presented as the dotted bar) and CO shift (presented as the solid bar). *OWGS on Rh: 30% of CO committed to CH_4 formation reaction ($2CO + 2H_2 = CH_4 + CO_2$).

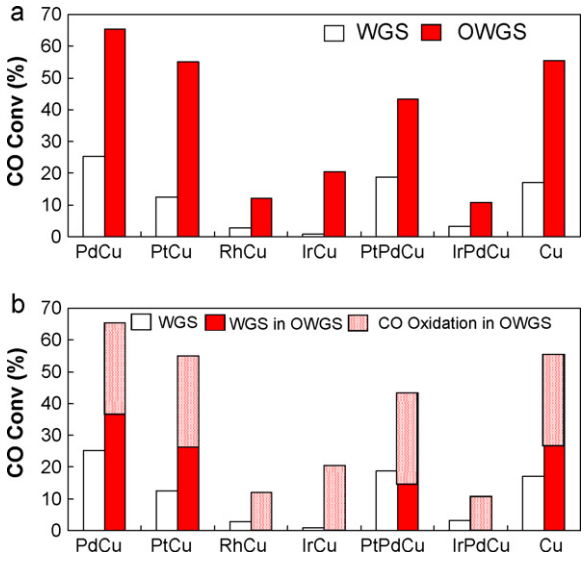

Fig. 2. (a) Screening test results for 1 wt% NM – 5 wt% Cu/CeO_2. Feed: 9.7% CO/22.8% H_2O/6.3% CO_2/37.9% H_2/6.9% N_2 or Air/argon balance, Temp = 260 °C, GHSV = 64,400 h^{-1}(dry); Each NM is 1 wt% for bimetallic and trimetallic catalysts. (b) The CO conversion for OWGS in (a) was divided into contributions of CO oxidation (28.9% of CO conv., presented as the dotted bar) and CO shift (presented as the solid bar).

O_2 assuming all of O_2 was consumed for CO oxidation. Since some amount of O_2 may be consumed for H_2 combustion, contribution by WGS in OWGS would be higher than calculated value shown in Fig. 1b. The results indicate that both WGS and OWGS activities are strongly dependent on metal species. OWGS generally gave higher CO conversion than WGS (Fig. 1a), but if the contribution by CO oxidation was subtracted, CO shift to H_2 in OWGS was only slightly higher or lower than that in WGS for monometallic series (Fig. 1b). Platinum is most active among noble metals, which is consistent with many reports [26,27]. Rhodium and iridium showed only CO oxidation activity in OWGS condition and nearly no activity for WGS (Fig. 1b). Rh also showed significant methanation activity under OWGS condition. Palladium was much less active compared to other noble metals in OWGS, meaning O_2 in the OWGS feed is more consumed for combustion of H_2. In CO oxidation, Pd on ceria exhibits high performance [28]. The low selectivity towards CO oxidation with monometallic Pd catalyst probably originates from its higher affinity towards hydrogen as it is also observed in the permeation of hydrogen through Pd membrane [29,30]. Nonetheless, the Pd catalyst exhibited certain WGS activity unlike Rh and Ir. Zhao and Gorte observed that WGS activity of Pd/CeO_2 catalyst was further improved by addition of iron [31], which indicates there is potential for improving monometallic catalysts by modification of its structure or electronic state.

Among the base metals supported on CeO_2, Cu is the only one that exhibited promising activity for OWGS (Fig. 1a) and WGS (Fig. 1b). Other metals had CO oxidation activity with good selectivity, but little WGS activity (Fig. 1b). Nickel was not included in the figure since it produced significant amount of methane and the catalyst bed temperature was out of control due to the high exotherm of methanation reaction. Over all, Pt and Cu showed high OWGS activity. Pd, Pt, and Cu showed a certain WGS activity at the present condition and therefore have potential to be improved further.

Since Cu has the best activity among base metals, various combinations of Cu and noble metals (NMs) were explored in the next step. Fig. 2 shows the CO conversion over CeO_2-supported bimetallic and trimetallic catalysts in the same scale as Fig. 1. Fig. 2a presents the measured CO conversion over the catalysts, while Fig. 2b divides CO conversion in OWGS into two parts including the contribution of both WGS (CO shift) and CO oxidation (calculated from added O_2 assuming all of O_2 was consumed for CO oxidation). Among the tested, Pd–Cu and Pt–Cu combinations were better than monometallic Cu, Pd, or Pt catalysts (Fig. 2a). The Pd–Cu showed the best activity for both WGS and OWGS (Fig. 2a) and the CO shift reaction was significantly enhanced in OWGS (Fig. 2b). It is interesting to note Pd–Cu was better than Pt–Cu among bimetallic systems (Fig. 2) while Pt was better than Pd among monometallic systems (Fig. 1). For Pt–Cu, WGS activity was slightly lower than Cu, while OWGS over Pt–Cu was clearly more effective than Cu (Fig. 2b), suggesting addition of O_2 effectively enhances WGS on Pt–Cu. The Rh–Cu and Ir–Cu were much less active than Cu monometallic catalyst and the selectivity for CO oxidation in OWGS was also worse. Thus, Rh and Ir are considered to be inhibitors for Cu catalyst contrary to Pd and Pt cases. This is also corroborated by the fact that Ir–Pd–Cu trimetallic catalyst showed similar or even lower activity than Ir–Cu. Since both Pt and Pd have positive effect on Cu, the trimetallic catalyst, Pd–Pt–Cu/CeO_2, was also tested. However, the activity was lower than either Pd–Cu or Pt–Cu. The result was rather similar to Pd–Pt/CeO_2 (not shown in the figure). From these observations, it is concluded that the co-presence of Pd, Pt and Cu leads to emergence of only the surface property of Pt–Pd bimetal. Pd and Pt would be more miscible together than Cu since their bond distances are closer and therefore the unique environment created by Pd–Cu and Pt–Cu is probably lost in the co-presence of Pd and Pt in Cu.

The above results indicate that metal species have significant impact both on WGS and on OWGS activity. The active sites are sensitive to the metal composition and the addition of a third metal can easily destroy such active sites. Since Pd–Cu on CeO_2 showed strong synergistic effect and exhibited the best OWGS activity, the subsequent study will focus on the Pd–Cu bimetallic composition to optimize the metal loadings and to elucidate the mechanism of the synergistic effect in Pd–Cu combination.

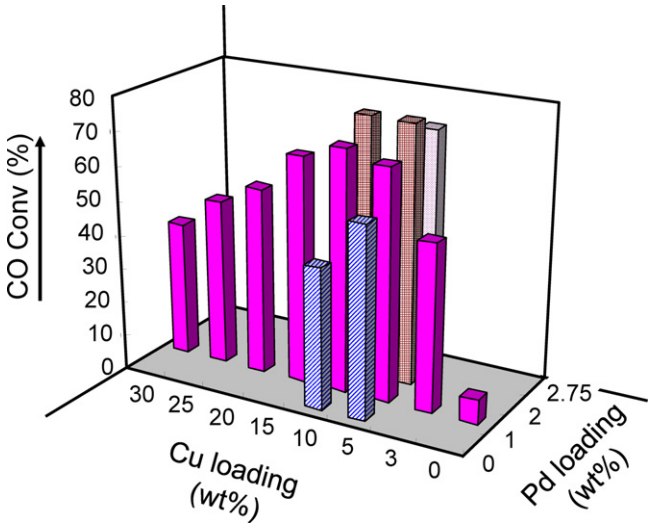

Fig. 3. Optimized Pd and Cu loadings for OWGS. Feed: 9.7% CO/22.8% H_2O/6.3% CO_2/37.9% H_2/6.9% N_2 or Air/argon balance, Temp = 260 °C, GHSV = 64,400 h^{-1} (dry).

3.2. Effect of metal loadings in Pd–Cu/CeO_2

To identify the best composition for Pd–Cu/CeO_2 catalyst in the present reaction condition, both Pd and Cu loadings were changed and their OWGS activities are compared in Fig. 3. When Pd loading was fixed to 1 wt%, addition of only 3% of Cu to Pd/CeO_2 enhanced CO conversion significantly. This indicates that the presence of Cu is crucial for high OWGS activity. The CO conversion increased with increasing Cu content till 10 wt% of loading and further increase of Cu caused decrease of CO conversion. The existence of the maximum performance with certain Cu content indicates there is an optimum amount of finely dispersed Pd–Cu species on CeO_2 and the excess amount of Cu would cause the increased size of the metal species. High Cu loading in Pd–Cu would also change the electronic structure of bimetallic species towards that of monometallic Cu. The better activity for 10 wt% of Cu loading for Pd–Cu catalyst than the 5 wt% Cu loading in contrast to the inverse trend for monometallic Cu catalyst suggest the Cu or Pd–Cu species are kept more dispersed in the presence of Pd.

When Cu loading was fixed to 5 wt%, CO conversion increased with increasing Pd loading. The activity reached maximum at 2 wt% Pd and further increase of Pd led to decrease of activity. Compared to the increase of Cu loading from 5% to 10%, OWGS activity was much more enhanced by the increase of Pd loading from 1% to 2%. This large impact of Pd loading on OWGS activity suggests that Pd is still highly dispersed in Cu in Pd(2)Cu(5)/CeO_2. In fact, the EXAFS result in Fig. 6 reveals that Pd atoms are mainly surrounded by Cu atoms in Pd–Cu and there is little Pd–Pd bonding in this catalyst. These observations suggest Pd and Cu makes well-mixed alloy in a wide range of metal loadings while the size of the alloy is sensitive to metal loadings and therefore influential to activity. The optimum Pd–Cu/CeO_2 catalyst composition was identified to be around 2% Pd and 5% Cu.

3.3. TPR and OSC studies

The effects of Pd and Cu loadings on reducibility of catalysts were investigated by TPR for Pd–Cu/CeO_2 system. In Fig. 4a, TPR profiles for different Cu loadings in the presence and absence of 1 wt% Pd and those of different Pd loadings in the presence of 5 wt% Cu are compared. Inside the parenthesis in the figure shows H_2 uptake calculated from peak area relative to that of pure CuO (Fig. 4b). Reduction temperature and H_2 uptake are summarized in Table 1.

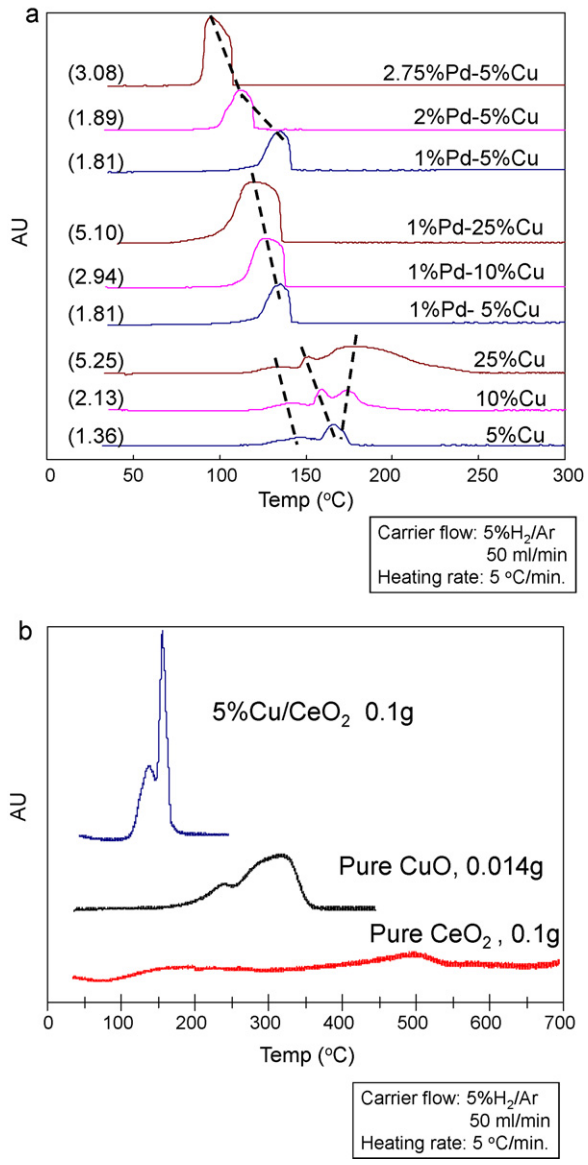

Fig. 4. (a) Effect of metal loadings on temperature programmed reduction (TPR) of Pd–Cu/CeO_2 catalysts. TPR condition: 50 ml/min of 5% H_2/Argon flow, 5 °C/min of heating rate. Inside parenthesis shows H_2 uptake in the unit of mmol/g. (b) Comparison of temperature programmed reduction (TPR) of pure CeO_2, CuO, and Cu/CeO_2. TPR condition: 50 ml/min of 5% H_2/Argon flow, 5 °C/min of heating rate.

The 5 wt% Cu/CeO_2 had only two peaks which are assigned to dispersed CuO particles [32–37]. These two species could be further assigned to CuO clusters and ionic Cu directly interacting with ceria according to the literature [32,38]. The H_2 uptake for this catalyst was 1.36 mmol H_2/g. If the catalyst is assumed to be completely in oxidized state before reduction, H_2 uptake by CeO_2 surface is estimated to be 586 μmol H_2/g, which was close to surface oxygen

Table 1
Reduction temperature and H_2 uptake in TPR of Pd–Cu catalysts with various metal loadings.

Catalyst	Cu/Pd ratio	Red. temp (°C)	H_2 uptake (mmol/g)
Cu(5)/CeO_2	–	138,165	1.36
Pd(1)Cu(5)/CeO_2	8.2	135	1.81
Pd(2)Cu(5)/CeO_2	4.1	115	1.89
Pd(2.75)Cu(5)/CeO_2	3.0	96	3.08
Pd(1)Cu(10)/CeO_2	16.4	128	2.94

Reduction condition: 50 ml/min of 5% H_2/Argon flow, 5 °C/min of heating rate.

reduction of pure CeO_2 (566 μmol H_2/g, Fig. 4b). The samples with Cu loading higher than 10 wt% showed another peak at higher temperature, which is assigned to the reduction of bulk CuO species. The reduction temperature of the bulk CuO is still much lower than that of bulk CuO without support, which usually takes place at above 200 °C [39], meaning even bulk copper is under strong influence on CeO_2. As Cu loading increases, the former two peaks shifted to lower temperature while the third peak shifted towards higher temperature, whose intensity drastically increased also. The observed behaviors of three CuO species is reasonable since small CuO particles would be in good contact with CeO_2 support and bulk CuO particles would become more isolated as Cu loading increase [40]. The negative influence of increased Cu loading on catalytic activity in Fig. 3 clearly shows negative effect of bulk Cu species to the catalytic reaction. Contrary to the monometallic series, bimetallic series containing 1 wt% Pd had somewhat broad single peak for all the cases. More importantly, the reduction temperature shifted towards lower temperature with increasing Cu loading, which is in sharp contrast to the trend observed for bulk CuO species in monometallic Cu/CeO_2. The result clearly shows that loading of only 1 wt% Pd significantly changes the reducibility of CuO species especially that of bulk CuO. The similar shape of the reduction peaks in various Cu/Pd ratios indicates fairly homogeneous alloy can form in a wide Cu/Pd range. These reduction characteristics are well consistent with the EXAFS results in the later section that proved alloy formation between Pd and Cu. The bell-shaped peak of the bimetallic catalysts allows us to speculate that Pd–Cu alloy has some variation in structure or composition in microscopic level, i.e. disordered alloy with short-range ordering or $PdCu_x$ composition with certain range in "*x*". During the reduction, alloy could be continuously restructured. The tail of the peak in low temperature side and the clear end of reduction process at high temperature side also implies the restructuring of alloy during reduction.

The H_2 uptake for Pd(1)Cu(5)/CeO_2 was 1.81 mmol H_2/g and H_2 uptake by CeO_2 surface is estimated to be 955 μmol H_2/g if the catalyst is assumed to be completely oxidized state before reduction. Compared to 586 μmol H_2/g of H_2 uptake by CeO_2 on Cu(5)/CeO_2, it is obvious that Pd makes catalyst more deeply reduced. It is also noted that with higher Cu loading (25 wt%), Pd–Cu bimetallic catalyst showed lower H_2 uptake than monometallic Cu probably because copper is partly reduced in Pd(1)Cu(25)/CeO_2 before reduction. Corresponding Ce^{3+} percentage in CeO_2 after reduction was estimated according to the following reaction equation:

$$CeO_2 + ½H_2 = ½Ce_2O_3 + ½H_2O \quad (R1)$$

Approximately 20.2% and 32.8% of Ce is present as Ce^{3+} in Cu(5) and Pd(1)Cu(5) catalysts, respectively. Compared to the reported Ce^{3+} percentage, 15.7% for co-precipitated 10 mol% Cu(10)–CeO_2 [41] and 23% for 1.45 wt% Rh/CeO_2 [42], the values in the present study are somewhat higher probably due to difference in metal species, surface area of CeO_2 support, and experimental conditions. The high Ce^{3+} percentage for the catalysts with high Cu loading was consistent with the report by Batista et al. who observed over 50% of CeO_2 partial reduction on 20 mol% CuO–CeO_2 catalyst even with about 30 m^2/g of surface area [41]. The Ce^{3+} percentage was 46% for Pd(1)Cu(10)/CeO_2 in the present study.

When Pd loading was increased with Cu loading fixed to 5 wt%, the reduction temperature significantly shifted towards lower side. The shift of reduction peak was much larger than the case in which Cu loading was changed. The reduction took place at less than 100 °C on Pd(2.75)Cu(5)/CeO_2. This large influence of Pd loading on reducibility shows larger driving force of Pd to reduce the catalyst. Also, alloy formation could be thermodynamically favored with increased Pd loading. In fact, there are two stoichiometric alloy compositions, $PdCu_3$ and PdCu, and meta-stable disordered structures are formed in a wide range of Cu/Pd ratio (10–25 at% of Pd, i.e. 9–3 of Cu/Pd ratio for the stoichiometric $PdCu_3$ region and most stable composition lies at around 15–20 at% Pd, i.e. 5.7–4.0 of Cu/Pd ratio) [47]. In the present study, Cu/Pd ratio is 8.4, 4.2, 3.0 for 1, 2, 2.75 wt% of Pd loading, respectively, and the catalysts with 2 wt% Pd loadings are closest to the most stable alloy structure. The reduction peak of Pd(2.75)Cu(5)/CeO_2 catalyst had relatively clear start and end of reduction. The defined reduction peak of this sample indicates more ordered fractions in the alloy.

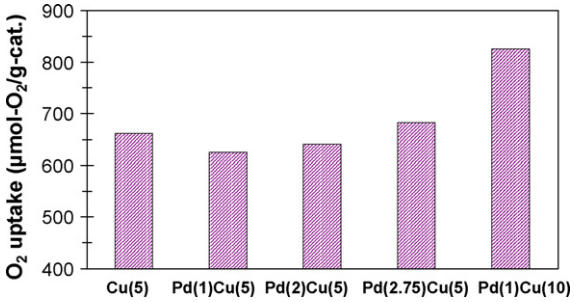

Fig. 5. Effect of metal loadings on oxygen storage capacity (OSC) of Pd–Cu/CeO_2 catalysts. Measurement temperature: 260 °C. Air pulses were submitted to the catalysts prereduced at 260 °C.

The effect of Pd content on physicochemical properties was further investigated by measuring oxygen storage capacity (OSC). The OSC was measured according to the method in the literature [43] except that the temperature of interest in the present study was 260 °C, i.e. the sample was reduced in H_2 at 260 °C, followed by air pulses in argon at the same temperature. In Fig. 5 and Table 2, total O_2 uptake is presented. O_2 uptake on 5% Cu monometallic catalyst (663 μmol O_2/g cat.) corresponds to about the half of H_2 uptake in TPR (1.36 mmol H_2/g cat.), indicating the catalyst is almost oxidized to the original oxidation state by air pulse at 260 °C. Compared to literature [44], the O_2 uptake was 1.5 times higher than 10 at% Cu–CeO_2–La_2O_3, but considering the difference in tested temperature (260 °C and 200 °C), metal loading (5 wt% and 3.9 wt%), preparation method (impregnation and urea gelation method), the obtained value is reasonable. The Pd–Cu bimetallic catalysts showed lower OSC (626 μmol O_2/g cat.) than 5 wt% Cu monometallic catalyst regardless of its higher H_2 uptake in TPR (1.81 mmol H_2/g cat.). This would be because the bimetallic catalysts are more reduced and resistant towards oxidation, which could be indicative of less pyrophoric nature. Difficulty in complete reoxidation of metal-loaded CeO_2 has also been pointed out by Fallah et al. [42]. An irreversible surface change on Au–CeO_2 in TPR was also reported by Deng et al. [45]. Our previous XPS study has proven that the surface is more reduced on the bimetallic catalyst than monometallic Cu catalyst [10].

The obtained OSC values, 600–700 μmol O_2/g cat. or 1200–1400 μmol O/g cat., were higher than the OSC of 3% Pt/CeO_2 catalysts with similar surface area (about 600 μmol O/g cat.) reported by Holmgren et al. [46]. Sharma et al. also reported about 850 μmol O/g cat. of OSC for monometallic 1% Pd/CeO_2 catalyst

Table 2
Physicochemical properties of Pd–Cu catalysts with various metal loadings.

Catalyst	BET (m^2/g)	O_2 uptake (μmol O_2/g)
Cu(5)/CeO_2	136	663
Pd(1)Cu(5)/CeO_2	132	626
Pd(2)Cu(5)/CeO_2	115	642
Pd(2.75)Cu(5)/CeO_2	115	683
Pd(1)Cu(10)/CeO_2	106	825
[a]Pd(1)Cu(30)/CeO_2	97	–
[a]Cu(30)/CeO_2	62	–

[a] BET surface area from the literature [11].

Table 3
Fitted parameters from EXAFS for various catalysts.

Sample	Scatter	N	R, Å	DWF ($\times 10^3$)	E_o, eV	Est. size
Pd foil	Pd–Pd	12	2.75			Large
[a]Pd(1)/CeO_2	Pd–Pd	5.7	2.71	5.0	−2.2	15 Å
Pd(2)Cu(5)/CeO_2	Pd–Cu	7.1	2.59	2.0	−4.9	Cu-rich bimetallic
	Pd–Pd	1.4	2.73	2.0	−1.0	
Pd(2.75)Cu(5)/CeO_2	Pd–Cu	7.1	2.59	2.0	−4.0	Cu-rich bimetallic
	Pd–Pd	1.7	2.73	2.0	−1.0	
[b]Cu foil	Cu–Cu	12	2.55			
Cu(5)/CeO_2	Cu–Cu	5.0	2.51			
[a]Cu(30)/CeO_2	Cu–Cu	8.9	2.55	0.1	0.3	
[c]Pd(2)Cu(5)/CeO_2_Air	Cu–O	4.0	1.92	2.7	−11.3	Cu^{2+}
Pd(2)Cu(5)/CeO_2	Cu–Cu	6.8	2.54	4.0	−2.5	Cu–Pd bimetallic
	Cu–Pd	2.0	2.64	4.0	6.7	40 Å
[b]Pt foil	Pt–Pt	12	2.77			
Pt(1)/CeO_2	Pt–Pt	4.7	2.66	2.0	−5.5	11 Å
Pt(1)Cu(5)/CeO_2	Pt–Cu	5.8	2.54	2.0	1.7	Cu-rich bimetallic
	Pt–Pt	3.0	2.75	2.0	−1.0	

[a] From the literature [11].
[b] Theoretical values.
[c] Measured in air at room temperature.

[47]. The higher O_2 uptake observed in the present study would be due to high Cu loading compared to monometallic Pt or Pd in the literature. Corroborated with the estimated Ce^{3+} percentage from TPR, the extent of ceria reduction is dependent strongly on metal loading.

It should be noted that the effect of metal–support interaction is beyond the scope of the present study. In our previous work [10], in situ XPS has shown that loading Pd–Cu on CeO_2 significantly promotes reduction of Ce^{4+} to Ce^{3+} while CeO_2 support enhances CuO reduction at lower temperatures. Pd addition further promotes low-temperature reduction of CuO on CeO_2 [10]. As a result of the metal–CeO_2 interaction, Pd–Cu/CeO_2 shows higher catalytic activity for OWGS than Pd–Cu/Al_2O_3 under the same reaction conditions [11]. The present study at least shows the presence of only 1% Pd is enough for influencing the redox properties of both Cu and CeO_2.

3.4. Local structure (EXAFS) of Pd–Cu on CeO_2

The Fourier transform of Pd K-edge EXAFS spectrum for reduced Pd(2)Cu(5)/CeO_2 catalyst is shown in Fig. 6 along with that of Pd foil.

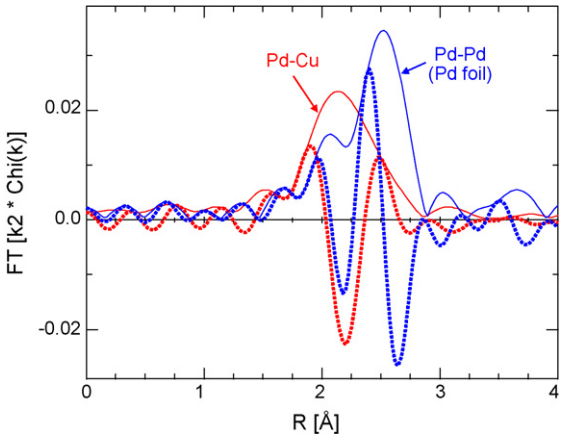

Fig. 6. Fourier transform of Pd EXAFS of Pd(2)Cu(5)/CeO_2 catalyst reduced at 250 °C. (k^2: Δk = 2.9–11.4 $Å^{-1}$). Blue solid: Pd foil data-magnitude of FT, N_{Pd-Pd} = 12.0 at 2.75 Å; blue dotted: Pd foil data-imaginary part of FT; solid red: Pd–Cu/CeO_2 data-magnitude of FT, N_{Pd-Cu} = 7.3 at 2.60 Å; red dotted: Pd–Cu/CeO_2 data-imaginary part of FT. (For interpretation of the references to color in this figure legend, the reader is referred to the web version of the article.)

Note that the structure did not change much in the condition with 1%CO–3%H_2O at 260 °C. Coordination numbers and bond distances were determined from fitting the magnitude and imaginary parts of the Fourier transform and these parameters are given in Table 3. The Pd foil showed two peaks, one large peak at about 2.5 Å (phase uncorrected distance) and one small peak at lower R that represent a single Pd–Pd scattering pair for 12 atoms at a bond distance of 2.75 Å. Pd foil is a face-centered cubic (FCC) crystal with a 3.89 Å lattice parameter. The Pd(2)Cu(5)/CeO_2 catalyst showed a single peak, but the position of the metallic peak is significantly shifted to lower bond distance from 2.75 Å of Pd foil to 2.59 Å indicating a different coordination environment around the Pd atoms. Fit of first shell peak in Pd(2)Cu(5)/CeO_2 indicates that (metallic) Pd has about 7 Cu neighbors with about 1.5 Pd neighbors, indicating that Pd is primarily coordinated to Cu atoms in a Pd–Cu alloy. The total coordination number was much smaller than that of FCC-type crystal, which suggests that either Pd–Cu alloy is highly dispersed, or Pd is located more on the surface of the alloy. The Pd(2.75)Cu(5)/CeO_2 catalyst, that has same Cu/Pd ratio as stoichiometric $PdCu_3$, basically showed identical EXAFS result. This indicates the Pd–Cu on CeO_2 is still a somewhat disordered alloy even with the Cu/Pd ratio identical to $PdCu_3$.

Compared with our previous report for Pd(1)Cu(30)/CeO_2 (R_{Pd-Cu} = 2.55 and N_{Pd-Cu} = 4.0 [11]), both bond distance and coordination number of Pd–Cu bonding are larger in the present catalysts. In the former, the Cu to Pd ratio was sufficiently high that there was little evidence of a Pd–Pd scattering contribution. In addition, the low Pd coordination number indicates a much smaller size of the metallic particles with Pd. The shorter Pd–Cu bond distance is also consistent with this conclusion. With the higher Pd loading and much lower Cu to Pd ratio, the bimetallic particles in Pd(2)Cu(5)/CeO_2 are larger, the number of Cu neighbors is higher and the bond distance increases. In addition, Pd has a few Pd neighbors which are not observed in the highly loaded Cu catalyst. From EXAFS analysis, however, one can conclude that Pd is highly dispersed in Cu to form Pd–Cu alloy.

Fig. 7 shows the Fourier transform of Cu-K-edge EXAFS of Pd(2)Cu(5)/CeO_2 before reduction in air atmosphere at room temperature. The peak at about 1.4 Å (not phase corrected) is due to Cu–O. The Cu–O bonds and bond distance are consistent with Cu^{2+}, e.g. CuO has 4 Cu–O at 1.95 Å while Cu_2O has 2 Cu–O at 1.85 Å. The higher shell Cu–O–Cu distance was at a position similar to the higher shell of CuO, which confirms TPR results. The

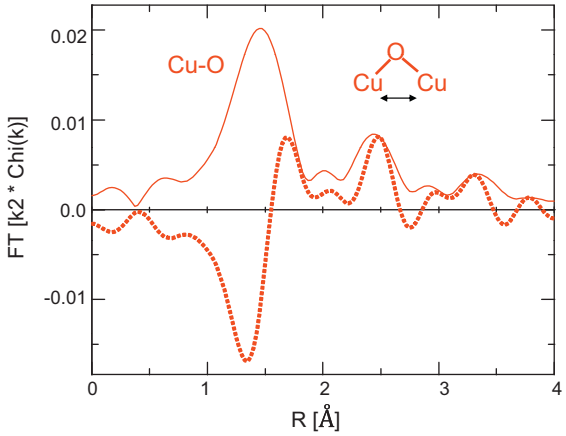

Fig. 7. Fourier transform of Cu EXAFS of Pd(2)Cu(5)/CeO_2 catalyst in air at room temperature. (k^2: Δk = 2.7–10.7 Å^{-1}). Red solid: Pd–Cu/CeO_2 data-magnitude of FT, N_{Cu-O} = 4 at 1.92 Å; red dotted: Pd–Cu/CeO_2 data-imaginary part of FT. (For interpretation of the references to color in this figure legend, the reader is referred to the web version of the article.)

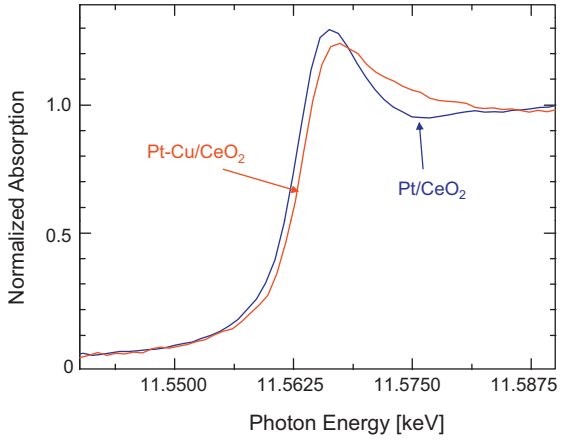

Fig. 9. Pt L_3-edge XANES of Pt(1)/CeO_2 and Pt(1)Cu(5)/CeO_2 reduced at 250 °C. Blue: Pt/CeO_2, red: Pt–Cu/CeO_2. (For interpretation of the references to color in this figure legend, the reader is referred to the web version of the article.)

Cu in the oxidized catalyst exists as CuO monoclinic structure. Fig. 8 shows the Cu K-edge magnitude and imaginary part of the Fourier transform of reduced Pd(2)Cu(5)/CeO_2 catalyst and Cu foil. Upon reduction of the catalyst, Cu was completely reduced. The EXAFS fits of the first shell (given in Table 3) gave a bond distance of 2.54 Å consistent with FCC metallic Cu. The asymmetry of the imaginary part of the Fourier transform indicates a second scatter at longer bond distance, indicating a Cu–Pd scattering contribution. The coordination number of Cu–Cu was 6.8 while that of Cu–Pd was 2.0. For the Pd(1)Cu(30)/CeO_2 sample in the previous work there is no clear indication of Pd neighbors from the Cu edge due to its high Cu content (30 wt%), but the Pd neighbors are visible in the catalyst in the present study. The percentage of Cu–Cu neighbors out of total coordination number was 77%, higher than 66% for stoichiometric $PdCu_3$, which is reasonable for Cu-rich non-stoichiometric alloy. An estimate of the particle size from the coordination number indicates that the metallic particle size is about 40 Å. The lower coordination number compared to Pd(1)Cu(30)/CeO_2 case in the previous study (N_{Cu-Cu} = ~10, average particle size was about 55 Å) also confirms the smaller alloy particle in the present catalyst compared to bulk Cu present in high Cu loading sample in the previous study.

Figs. 9 and 10 show Pt L_3 XANES and Pt L_3 EXAFS Fourier transform of Pt(1)Cu(5)/CeO_2 in comparison to Pt(1)/CeO_2. The significant shift in the edge position within the range from 11.54 to 11.59 keV and change of shape of the XANES are indicative of Pt–Cu alloy. The EXAFS fits of the first shell are given in Table 3. The Pt/CeO_2 has very small particles with a shortened Pt bond distance (2.66 Å against 2.77 Å for Pt Foil). Similar decrease in the bond distance has been observed in Pd/CeO_2 [11] wherein the Pd bond distance was 2.71 Å compared to 2.75 Å in Pd foil and N_{Pd-Pd} was 5.7. Similar contraction of the metal–metal bond distance has been reported for Au catalysts [48]. It is inferred that Pt is more easily dispersed on CeO_2 so that Pt bond distance is more contracted. Although the Cu/M ratio of Pt(1)Cu(5)/CeO_2 is four times of that in Pd(2)Cu(5)/CeO_2, there are more Pt–Pt neighbors than Pd–Pd neighbors. The Pt coordination environment in Pt(1)Cu(5)/CeO_2, is 6 Cu neighbors at 2.54 Å and 3 Pt neighbors at 2.75 Å. The high N_{Pt-Pt} in Pt(1)Cu(5)/CeO_2 compared to N_{Pd-Pd} in Pd(2)Cu(5)/CeO_2 clearly shows less miscible property of Pt into Cu compared to Pd into Cu. The better alloy formation in Pd–Cu may be one of the factors for better catalytic activity.

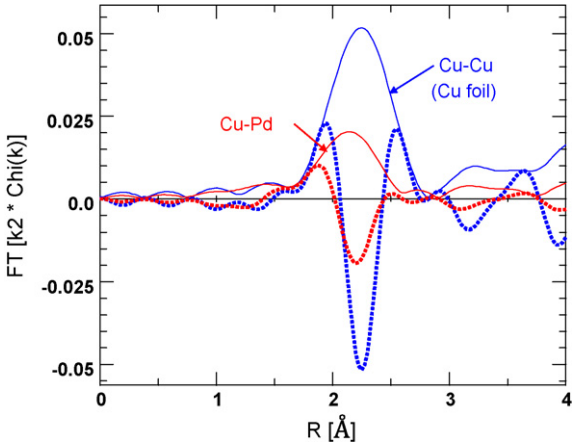

Fig. 8. Fourier transform of Cu EXAFS of Pd(2)Cu(5)/CeO_2 catalyst reduced at 260 °C. (k^2: Δk = 2.7–11.0 Å^{-1}). Blue solid: Cu foil data-magnitude of FT, N_{Cu-Cu} = 12 at 2.55 Å; blue dotted: Cu foil data-imaginary part of FT; red solid: Pd–Cu/CeO_2 data-magnitude of FT, N_{Cu-Cu} = 6.8 at 2.54 Å, N_{Cu-Pd} = 2.0 at 2.64 Å; red solid: Pd–Cu/CeO_2 data-imaginary part of FT. (For interpretation of the references to color in this figure legend, the reader is referred to the web version of the article.)

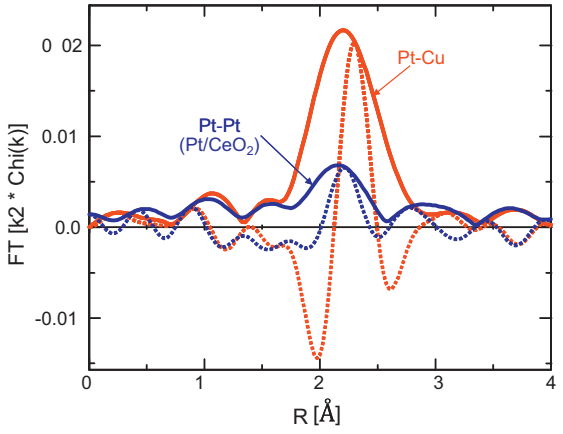

Fig. 10. Fourier transform of Pt EXAFS of Pt(1)/CeO_2 and Pt(1)Cu(5)/CeO_2 catalysts reduced at 250 °C. (k^2: Δk = 2.8–10.2 Å^{-1}). Blue solid: Pt/CeO_2 data-magnitude of FT, N_{Pt-Pt} = 4.7 at 2.66 Å; blue dotted: Pt/CeO_2 data-imaginary part of FT; red solid: Pt–Cu/CeO_2 data-magnitude of FT, N_{Pt-Cu} = 5.88 at 2.54 Å, N_{Pt-Pt} = 3.0 at 2.75 Å; red dotted: Pt–Cu/CeO_2 data-imaginary part of FT. (For interpretation of the references to color in this figure legend, the reader is referred to the web version of the article.)

Table 4
Comparison of catalytic reaction rates and E_a values with the literature.

Catalyst	SA, m^2/g	T, °C	Feed gas, $CO/H_2O/CO_2/H_2$	Rate, μmol/s/g cat.	E_a, kJ/mol	Reaction order, $CO/H_2O/CO_2/H_2$	Ref.
$Pd(2)Cu(5)/CeO_2$	155	260	OWGS, $O_2/CO = 0.14$, 9.8/23/0/0	228	21.7	[a]1.4/0.3/–/–	This work
$Pd(2)Cu(5)/CeO_2$	155	260	9.8/23/0/0	142	56.9	[a]0.4/0.3/–/–	This work
$Pd(2)Cu(5)/CeO_2$	155	260	9.8/23/6.5/38.4	31.6			This work
$Pt(1)/CeO_2$	155	260	9.8/23/6.5/38.4	10.7			This work
Cu(5 at%)–Ce(La)O_2	100	250	1/2/0/0	3.7	[b]19.2–30.4		[54]
$Cu(8)/CeO_2$	180	200	7/8.5/22/37	0.11	56	0.9/0.4/−0.6/−0.6	[61]
Cu(10 at%)–CeO_2	[c]22.7	350	1/3/0/0		51		[18]
$Pd(1)/CeO_2$	30	240	3.2/4.2/1.3/1.3	~0.8	46	0/0.5/−1/−0.5	[24]
$Pd(1)/CeO_2$	61	180	3.3/3.3/0/0	0.45	49		[31]
Pt(2)/Ce–Zr	200	240	4.9/33/10.5/30.3	~13	71	0.07/0.67/−0.16/−0.57	[25]
$Pt(1)/CeO_2$	161	200	7/22/8.5/37	0.59	75	−0.03/0.44/−0.09/−0.38	[53]
Pt(3.7 at%)/Ce(La)O_2	150	250	11/26/7/26	~13	74.8		[52]

From the left column: catalyst, surface area of support, temperature, feed gas composition balanced by inert gas, reaction rate obtained or calculated from the literature, activation energy, reaction order, and reference number.
[a] The value obtained using $Pd(1)Cu(5)/CeO_2$ catalyst.
[b] Depends on the condition.
[c] Surface area of the catalyst.

3.5. Kinetic studies

To investigate how Pd and Cu loadings affects OWGS activity and how the combination of these two metals enhances the reaction, a kinetic study was conducted. The space velocity was set for complete O_2 consumption to highlight the effect of O_2 on H_2 production. For this reason, CO conversion in OWGS was obtained under differential condition but still far below equilibrium. Mass transport limitation was very small from rough calculation of Thiele modulus:

$$\varphi = R\left(\frac{k}{D_e}\right)^{1/2} \quad (1)$$

where k is rate constant, D_e is effective diffusion coefficient, and R is radius of catalyst particle. With 10^2 per site per second of CO oxidation rate achievable for stoichiometric CO/O_2 ratio on noble metal single crystal at around 250 °C [49] (20–200 per site per second of rate available at 250–300 °C on Pd/CeO_2 if 10% Pd dispersion [50]), 0.25–0.5 mm of particle size, approximately 0.8 cm^2/s of molecular diffusion coefficient for air, and 5.5 cm^2/s for H_2, Thiele modulus is 0.053–0.28. The corresponding effectiveness factor is 0.9948–0.9998, close to unity enough to ignore mass transport limitation.

3.5.1. Effect of O_2 addition

Fig. 11 presents Arrhenius plots for OWGS and WGS on $Pd(2)Cu(5)/CeO_2$ catalyst in the temperature range of 220–280 °C. The advantage of OWGS over WGS is very clear from Fig. 11. The H_2 production rate in OWGS at 260 °C was 228 μmol/s/g cat., which is 1.5 times higher than that in WGS (142 μmol/s/g cat.). While lower temperature is preferable for the $CO–H_2O–O_2$ conditions, around 260 °C was optimum for the feed with H_2 and CO_2 ($CO–H_2O–CO_2–H_2–O_2$ condition) [51] because H_2 and CO_2 significantly inhibit the reaction at low temperature. The H_2 production rate in such condition was 40.2 and 31.6 μmol/s/g cat. for OWGS and WGS, respectively. To check the validity of reaction rate, rates with some catalysts in this study were compared with the values from the literature in Table 4. The WGS rate for $Pt(1)/CeO_2$ catalyst in the present study was approximately 11 μmol/s/g cat. (260 °C), which is close to those of published studies [25,52] (~13 μmol/s/g cat. at 240 °C and 250 °C, respectively). The rate in one report [53] was lower by an order of magnitude due to its low-temperature condition (200 °C). Thus, the rate in the present study is considered to be in reasonable range and therefore the great advantage of O_2 addition to WGS as well as the advantage of bimetallic $Pd–Cu/CeO_2$ over Pt/CeO_2 become clear.

The apparent activation energy calculated by the slope of Arrhenius plots in Fig. 11 was 56.9 and 21.7 kJ/mol for WGS and OWGS, respectively. Compared to WGS, the milder slope of Arrhenius plots for OWGS could reflect an increased H_2O activation through a lowered surface CO coverage by O_2 addition upon adding O_2, which is less influenced by temperature.

How O_2 addition to WGS promotes H_2 production is one of the issues in OWGS. Bunluesin et al. have implicated involvement of oxygen in CeO_2 in WGS by showing a significantly lowered WGS rate when CeO_2 support is calcinated at high temperature [20]. Other articles report that the phase comprising ceria surface and ionic species such as Pt–O–Ce or Au–O–Ce is responsible for WGS [52]. For $Cu–CeO_2$, Li et al. and Liu et al. implicated the presence of Cu^+ species at the interface with CeO_2 in the form of Cu–O–Ce [54,55]. These reports show importance of oxygen at metal–ceria interface. O_2 addition to WGS could directly affect such sites. Meanwhile, some literature points out that catalyst surface is covered by chemisorbed CO island and the rate of CO oxidation is significantly limited by available sites for chemisorption of the coreactant [56,57]. The enhanced H_2 production by O_2 addition could be explained by removal of CO covering the surface to free up the active sites for WGS.

To investigate whether O_2 creates new active sites, the WGS rate of the catalysts pretreated by O_2 and pretreated by H_2 were

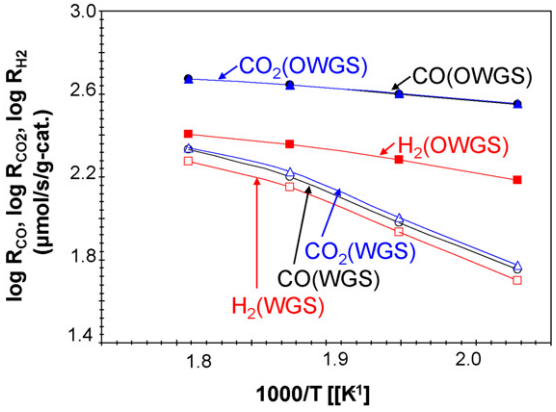

Fig. 11. Arrhenius plot of the rates of CO conversion, CO_2 production, and H_2 production on $Pd(2)Cu(5)/CeO_2$ catalyst. The rate of CO conversion in OWGS: filled circle; in WGS: open circle; the rate of CO_2 production in OWGS: filled triangle; in WGS; open triangle; the rate of H_2 production in OWGS: filled square; in WGS: open square. Gas composition: 9.8%CO/23.0% H_2O/6.9% air/N_2 balance; Amount of catalyst: 0.015 g (35–60 mesh) diluted with SiC particles of the same size to attain 0.065 ml of the catalyst bed volume. Temperature range: 220–280 °C.

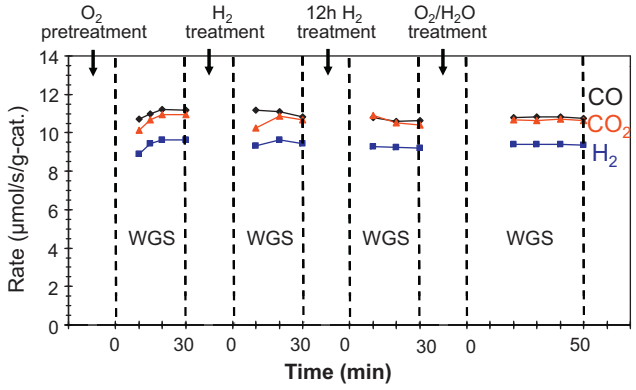

Fig. 12. Effect of O_2 pretreatment and H_2 pretreatment on WGS rate. Catalyst: Pd(1)Cu(5)/CeO_2 0.1 g, Feed: 9.8%CO/23.0% H_2O/N_2 balance; Temperature: 260 °C; GHSV: about 12,000 h^{-1} (on the CO basis). The conditions for O_2 and H_2 pretreatments were (1) pure air for an hour, (2) 50% H_2/N_2 for an hour, (3) 10% H_2/N_2 for about 12 h, and (4) 6.9% air/22.8% H_2O/N_2 for an hour, respectively.

measured and the results are shown in Fig. 12. The rates of H_2 production in WGS with O_2 pretreatment, H_2 pretreatment and with repeated O_2 pretreatment are similar, and the rates of CO_2 production nearly overlap with those of CO consumption in general. The catalyst initially pretreated by O_2 showed a slightly lower H_2 production rate, which then increased and within 10 min reached a steady state similar to or only slightly higher than that with H_2 pretreatment. These results clearly rule out the possibility that some "different and more active sites" were created by O_2 treatment or that the "O_2-treatment-induced different active sites" disappear quickly upon switching off O_2. Clearly, the major enhancement in H_2 production observed in OWGS (Fig. 11) compared to WGS was not observed in the WGS over O_2-pretreated catalyst (Fig. 12). Thus, it is concluded that the greatly enhanced H_2 production in OWGS (by O_2 addition to the WGS reaction system) is more relevant to change of surface dynamics involving co-reactants (CO, H_2O) rather than change of the nature of active sites on catalyst. WGS would be enhanced mainly by removing some chemisorbed CO by added O_2 to free up the active sites for H_2O chemisorption, although there is still a possibility that there are some differences in the active sites between the reaction systems with and without O_2 addition.

3.5.2. *Effect of metal loadings*

Fig. 13 shows the effects of Pd and Cu loadings on the rate of H_2 production in WGS and OWGS. The Arrhenius plots of OWGS/WGS on Pd(2)Cu(5) and Pd(1)Cu(10) are compared with Pd(1)Cu(5). In WGS, both increases of Pd and Cu caused higher H_2 production rate. The identical slope for the three catalysts in WGS means the higher rate is mainly by increase in the number of sites active for the reaction. In OWGS, the rates of H_2 production are higher than those in WGS for all the catalysts, particularly at lower temperatures. However, only the increase of Pd loading led to higher H_2 production rate in OWGS while the increase of Cu did not have a significant impact. The slopes were milder than those in WGS but similar for all the three catalysts. These behaviors show Pd and Cu loadings influence both the number and the property of active sites. The number of sites is increased both by Pd and by Cu addition, but the properties of the sites would differ and O_2 is more effectively utilized on the sites which Pd is involved in. Considering the Pd–Cu structure obtained in EXAFS study (Figs. 6 and 8), the number of

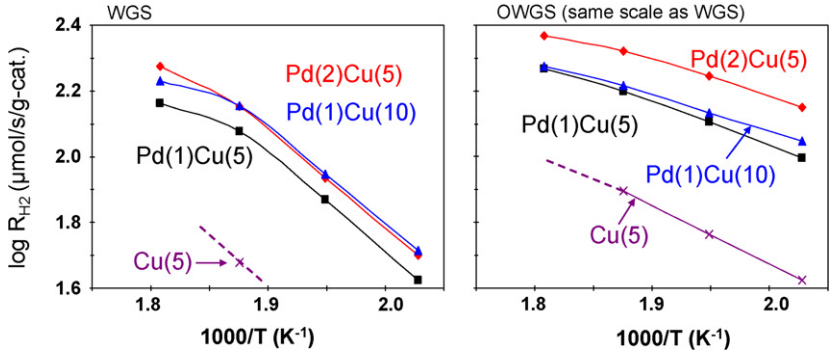

Fig. 13. Effect of metal loadings on H_2 production rate. Ceria-supported Pd(2)Cu(5): diamond; Pd(1)Cu(10): triangle; Pd(1)Cu(5): square; Cu(5): cross. Gas composition: 9.8%CO/23.0% H_2O/N_2 balance for WGS (left) and 9.8%CO/23.0% H_2O/6.9% air/N_2 balance for OWGS (right); Amount of catalyst: 0.015 g (35–60 mesh) diluted with SiC particles of the same size to attain 0.065 ml of the catalyst bed volume. Temperature range: 220–280 °C.

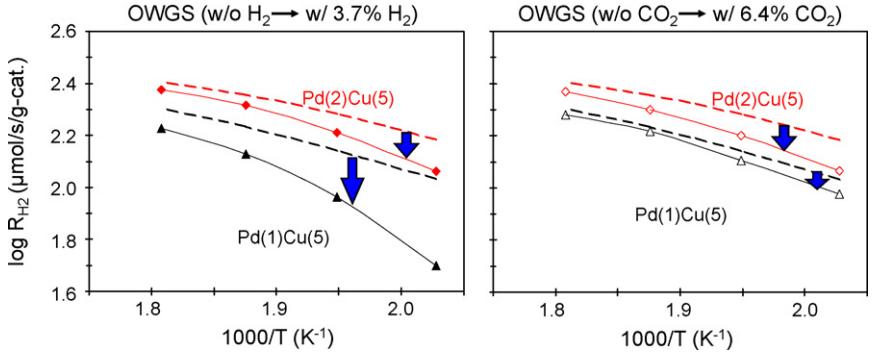

Fig. 14. Effect of metal loading in the presence and absence of the products (H_2 and CO_2) on H_2 production rate. Ceria-supported Pd(2)Cu(5): red diamond; Pd(1)Cu(5): black triangle. Dotted lines are the rate in OWGS in the absence of H_2 and CO_2 for the comparison with the solid lines. Gas composition: 9.8%CO/23.0% H_2O/6.9% air/N_2 balance. The N_2 concentration was adjusted upon addition of H_2 or CO_2 so that the total flow rate was kept constant. Amount of catalyst: 0.015 g (35–60 mesh) diluted with SiC particles of the same size to attain 0.065 ml of the catalyst bed volume. Temperature range: 220–280 °C. (For interpretation of the references to color in this figure legend, the reader is referred to the web version of the article.)

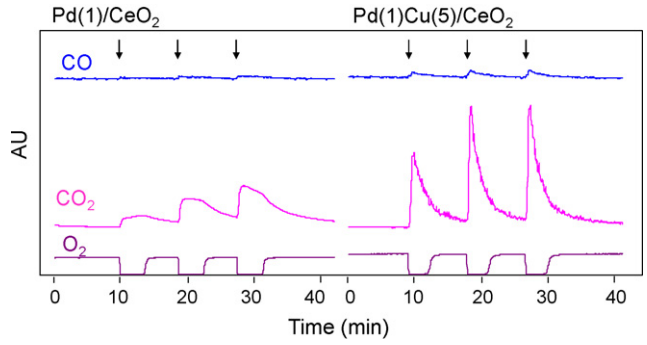

Fig. 15. Transient response to CO pulses on $Pd(1)/CeO_2$ and $Pd(1)Cu(5)/CeO_2$ at 260 °C. Carrier gas: 20 ml/min of 275 ppm O_2/Helium flow, pulse gas condition: 0.5 ml (heated at 110 °C) of 10% CO/Helium. The arrows show the timing of CO pulse injection.

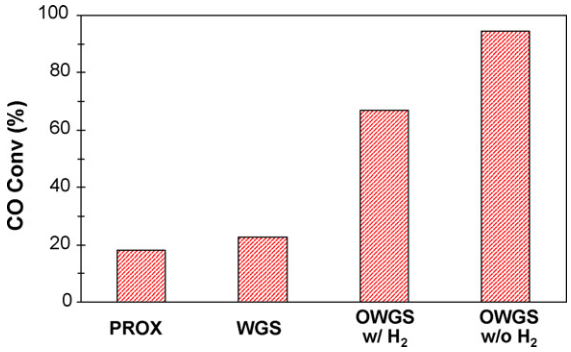

Fig. 16. Comparison of CO conversion level among PROX, WGS, and OWGS at 260 °C. Gas composition: 9.7% CO, 22.8% H_2O, 6.3% CO_2, 37.9% H_2, 1.4% O_2, N_2 or Ar balance for OWGS, 9.7% CO, 22.8% H_2O, 6.3% CO_2, 37.9% H_2, N_2 or Ar balance for WGS, and 9.7% CO, 6.3% CO_2, 37.9% H_2, 1.4% O_2, N_2 or Ar balance for PROX; GHSV: 64,400 h^{-1}(dry); Catalyst: $Pd(1)Cu(5)/CeO_2$.

adjacent Pd–Cu pairs would increase only by Pd addition and these sites might be specifically relevant to OWGS.

Change in site property with metal loading is also noted in the literature. A monometallic Pd/CeO_2 shows low PROX and WGS activities in contrast to high CO oxidation activity [29], which suggests monometallic Pd does not have selectivity to oxidize CO resulting in loss of H_2 by oxidation in the presence of O_2. Affinity of Pd towards hydrogen is well known and is made use for H_2 separation through membranes. When Pd forms alloy with Cu, the membrane shows lower hydrogen solubility compared to pure Pd [58] while Pd–Cu alloy keeps high selectivity and permeability of hydrogen [59,60]. Thus, the Pd–Cu alloy structure suppresses H_2 activation which is inherent to Pd alone.

Fig. 14 shows the effect of the presence of H_2 and CO_2 in the feed gas on the OWGS rates for Pd–Cu catalysts with 1 wt% and 2 wt% of Pd loading. Upon the addition of H_2 in the feed gas, the H_2 production rate decreased on both catalysts, but the extent of decrease was much smaller on Pd(2)Cu(5). At lower temperature, the larger inhibition by H_2 was observed. Since selective CO oxidation favors low temperature, the large drop of the rate at low temperature would be attributed to inhibition of H_2O dissociation by hydrogen:

$$H_2O = H(a) + OH(a) \quad (R2)$$

$$OH(a) = H(a) + O(a) \quad (R3)$$

The smaller drop of the rate on Pd(2)Cu(5) suggests that H_2 production is facilitated by the increase of Pd loading more pronouncedly in the presence of H_2, particularly at low temperature. The Pd addition would change the property of active sites for better H_2O activation.

When CO_2 was added to the feed gas, the H_2 production rate again decreased on both catalysts. However, contrary to the case of H_2 addition to the feed, decrease of the rate was larger on Pd(2)Cu(5) than Pd(1)Cu(5). The Pd addition possibly inhibits desorption of CO_2 from the catalyst surface (see Fig. 15). Note that the slope does not change as much as the case of H_2 addition, indicating reaction is inhibited by CO_2 equally in a wide temperature range.

Fig. 15 presents the transient pulse response signals of CO, CO_2, and O_2 to CO pulses in 275 ppm O_2 flow. Both Pd/CeO_2 and $Pd–Cu/CeO_2$ catalysts adsorbed most of the pulsed CO, accompanying CO_2 desorption and O_2 uptake at the same time. The O_2 uptake (represented by decreased O_2 level) continued for certain duration until the catalyst recovered its original oxidation state while CO_2 response underwent a maximum peak. The CO_2 desorption speed was faster on the Pd–Cu catalyst than that of monometallic Pd catalyst. The Pd–Cu was saturated with CO_2 in the second pulse while Pd catalyst did not saturate after the third pulse. These transient responses show Pd catalyst strongly retains CO_2 on its surface, possibly as carbonate, and the presence of Cu facilitates desorption of CO_2.

In summary for this section, Pd in Pd–Cu contributes more to active sites for H_2O activation with low inhibition by H_2. Pd also accompanies strong retention of CO_2 on the catalyst surface. Meanwhile, Cu in Pd–Cu facilitates CO_2 desorption. Cu also suppresses H_2 activation (for H_2 oxidation) inherent to Pd. From EXAFS, TPR, and OSC, Pd stabilizes Cu in alloy in reduced state and Cu disperses Pd in the alloy structure. Thus, Pd and Cu have complementary roles for fast CO shift to H_2.

Fig. 16 compares conversion levels between PROX, WGS, OWGS in the presence of H_2, and also OWGS in the absence of H_2 at 260 °C. PROX exhibited about 20% of CO conversion which corresponds to about 60–70% of CO oxidation selectivity. The rest of O_2 was consumed for H_2 combustion. WGS had slightly higher CO conversion than PROX. CO conversion in OWGS was much higher than WGS and PROX, even higher than the sum of CO conversions of WGS and PROX.

These results clearly indicate that OWGS is not simply the addition of oxidation reaction to WGS reaction. In the absence of H_2, CO conversion was further increased to reach 94%. As indicated in the above results, adding a small amount of O_2 changes the catalyst surface dynamics for H_2O activation to enhance WGS.

4. Conclusion

The metallic formulation of CeO_2 supported catalyst was found to strongly influence catalytic performance in oxygen-enhanced water gas shift (OWGS). Among the monometallic, bimetallic, and trimetallic catalysts examined, the Pd–Cu combination showed uniquely high activity in OWGS and the composition of 2 wt% Pd with 5–10 wt% Cu were found to be suitable for the present OWGS condition. The higher activity of the Pd–Cu catalyst was attributed to alloy structure and the accompanying synergistic interaction between Pd and Cu which was evidenced by TPR, OSC, and EXAFS.

The EXAFS study shows alloy formation between Pd and Cu on CeO_2. The Pd-edge showed Pd is mainly surrounded by Cu and Cu-edge clearly evidenced the existence of Cu–Pd bonding. The Pt-edge of $Pt–Cu/CeO_2$ catalyst exhibited higher number of Pt neighbors compared to the case of $Pd–Cu/CeO_2$, which indicates the better alloy formation in Pd–Cu than in Pt–Cu. This structural feature in Pd–Cu led to strong interaction between Pd and Cu as it was observed in TPR. All the Pd–Cu bimetallic catalysts with wide range of Pd and Cu loadings had a single reduction peak in contrast to multiple peaks observed for monometallic Cu catalyst. The OSC measurement showed Pd–Cu catalysts have stronger resistance towards air pulse oxidation than Cu monometallic catalysts, which

indicates Pd prevents oxidation of Cu in the alloy in the oxidative OWGS condition.

The kinetic study revealed that Pd loading also has a strong impact on H_2 production rate in OWGS. The presence of Pd in Pd–Cu was found to increase active sites for H_2O dissociation. The presence of Cu was found to suppress affinity of Pd towards hydrogen to prevent reaction inhibition by H_2 and suppress H_2 oxidation in OWGS. The presence of Cu in Pd–Cu was also shown to facilitate desorption of CO_2 which would otherwise attach to catalyst surface as carbonate.

The excellent OWGS activity of Pd–Cu catalysts has been attributed to these complementary roles of the two metals which would originate from alloy structure and strong interaction between them. The advantage of OWGS over WGS using Pd–Cu bimetallic catalyst supported on CeO_2 was clearly demonstrated in this study.

Acknowledgments

We wish to thank the US Office of Naval Research and the US Department of Energy-National Energy Technology Laboratory for partial support of the work on fuel processing for fuel cells. Use of the Advanced Photon Source is supported by the U.S. Department of Energy, Office of Science, and Office of Basic Energy Sciences, under Contract DE-AC02-06CH11357. MRCAT operations are supported by the Department of Energy and the MRCAT member institutions. We also thank Rhodia Co. for generously supplying CeO_2 support.

References

[1] C.S. Song, Catal. Today 77 (2002) 17–49.
[2] L.F. Brown, Int. J. Hydrogen Energy 26 (2001) 381–397.
[3] J.R. Rostrup-Nielson, T. Rostrup-Nielson, Cattech 6 (2002) 150–159.
[4] S. Velu, K. Suzuki, Top. Catal. 22 (2003) 235–244.
[5] A.F. Ghenciu, Curr. Opin. Solid State Mater. 6 (2002) 389–399.
[6] T.E. Springer, T. Rockward, T.A. Zawodzinski, S. Gottesfeld, J. Electrochem. Soc. 148 (2001) A11–A23.
[7] J. Larminie, A. Dicks, Fuel Cell Systems Explained, John Wiley & Sons, New York, NY, 2000.
[8] W. Ruettinger, O. Ilinich, R.J. Farrauto, J. Power Sources 118 (2003) 61–65.
[9] E.S. Bickford, S. Velu, C.S. Song, Catal. Today 99 (2005) 347–357.
[10] E.B. Fox, A.F. Lee, K. Wilson, C.S. Song, Top. Catal. 49 (2008) 89–96.
[11] E.B. Fox, S. Velu, M.H. Engelhard, Y.H. Chin, J.T. Miller, J. Kropf, C.S. Song, J. Catal. 260 (2008) 358–370.
[12] K. Sekizawa, S. Yano, K. Eguchi, H. Arai, Appl. Catal. A-Gen. 169 (1998) 291–297.
[13] G.C. Chinchen, M.S. Spencer, K.C. Waugh, D.A. Whan, J. Chem. Soc. Faraday Trans. I 83 (1987) 2193–2212.
[14] C. Rhodes, G.J. Hutchings, A.M. Ward, Catal. Today 23 (1995) 43–58.
[15] T. Utaka, K. Sekizawa, K. Eguchi, Appl. Catal. A-Gen. 194 (2000) 21–26.
[16] T. Utaka, T. Takeguchi, R. Kikuchi, K. Eguchi, Appl. Catal. A-Gen. 246 (2003) 117–124.
[17] R.J. Gorte, S. Zhao, Catal. Today 104 (2005) 18–24.
[18] H. Kusar, S. Hocevar, J. Levec, Appl. Catal. B-Environ. 63 (2006) 194–200.
[19] T. Bunluesin, H. Cordatos, R.J. Gorte, J. Catal. 157 (1995) 222–226.
[20] T. Bunluesin, R.J. Gorte, G.W. Graham, Appl. Catal. B-Environ. 15 (1998) 107–114.
[21] A. Martinez-Arias, M. Fernandez-Garcia, O. Galvez, J.M. Coronado, J.A. Anderson, J.C. Conesa, J. Soria, G. Munuera, J. Catal. 195 (2000) 207–216.
[22] Q. Fu, W.L. Deng, H. Saltsburg, M. Flytzani-Stephanopoulos, Appl. Catal. B-Environ. 56 (2005) 57–68.
[23] D. Andreeva, I. Ivanova, L. Ilieva, M.V. Abrashev, Appl. Catal. A-Gen. 302 (2006) 127–132.
[24] S. Hilaire, X. Wang, T. Luo, R.J. Gorte, J. Wagner, Appl. Catal. A-Gen. 215 (2001) 271–278.
[25] R. Radhakrishnan, R.R. Willigan, Z. Dardas, T.H. Vanderspurt, Appl. Catal. B-Environ. 66 (2006) 23–28.
[26] G. Jacobs, E. Chenu, P.M. Patterson, L. Williams, D. Sparks, G. Thomas, B.H. Davis, Appl. Catal. A-Gen. 258 (2004) 203–214.
[27] P. Panagiotopoulou, D.I. Kondarides, Catal. Today 112 (2006) 49–52.
[28] T. Bunluesin, E.S. Putna, R.J. Gorte, Catal. Lett. 41 (1996) 1–5.
[29] O. Pozdnyakova, D. Teschner, A. Wootsch, J. Krohnert, B. Steinhauer, H. Sauer, L. Toth, F.C. Jentoft, A. Knop-Gericke, Z. Paal, R. Schlogl, J. Catal. 237 (2006) 17–28.
[30] J.B. Hunter, Platinum Met. Rev. (1960) 130–131.
[31] S. Zhao, R.J. Gorte, Catal. Lett. 92 (2004) 75–80.
[32] L. Kundakovic, M. Flytzani-Stephanopoulos, Appl. Catal. A-Gen. 171 (1998) 13–29.
[33] W. Liu, M. Flytzani-Stephanopoulos, Chem. Eng. J. 64 (1996) 283–294.
[34] M.F. Luo, Y.J. Zhong, X.X. Yuan, X.M. Zheng, Appl. Catal. A-Gen. 162 (1997) 121–131.
[35] X.Y. Jiang, G.L. Lu, R.X. Zhou, J.X. Mao, Y. Chen, X.M. Zheng, Appl. Surf. Sci. 173 (2001) 208–220.
[36] J.B. Wang, S.C. Lin, T.J. Huang, Appl. Catal. A-Gen. 232 (2002) 107–120.
[37] T. Tabakova, F. Boccuzzi, M. Manzoli, J.W. Sobczak, V. Idakiev, D. Andreeva, Appl. Catal. A-Gen. 298 (2006) 127–143.
[38] G. Avgouropoulos, T. Ioannides, Appl. Catal. A-Gen. 244 (2003) 155–167.
[39] G. Fierro, M. Lojacono, M. Inversi, P. Porta, R. Lavecchia, F. Cioci, J. Catal. 148 (1994) 709–721.
[40] S.M. Zhang, W.P. Huang, X.H. Qiu, B.Q. Li, X.C. Zheng, S.H. Wu, Catal. Lett. 80 (2002) 41–46.
[41] P. Djinovic, J. Batista, A. Pintar, Appl. Catal. A-Gen. 347 (2008) 23–33.
[42] J. El Fallah, S. Boujana, H. Dexpert, A. Kiennemann, J. Majerus, O. Touret, F. Villain, F. Lenormand, J. Phys. Chem. 98 (1994) 5522–5533.
[43] H.C. Yao, Y.F.Y. Yao, J. Catal. 86 (1984) 254–265.
[44] Q. Fu, S. Kudriavtseva, H. Saltsburg, M. Flytzani-Stephanopoulos, Chem. Eng. J. 93 (2003) 41–53.
[45] W.L. Deng, J. De Jesus, H. Saltsburg, M. Flytzani-Stephanopoulos, Appl. Catal. A-Gen. 291 (2005) 126–135.
[46] A. Holmgren, B. Andersson, D. Duprez, Appl. Catal. B-Environ. 22 (1999) 215–230.
[47] S. Sharma, S. Hilaire, J.M. Vohs, R.J. Gorte, H.W. Jen, J. Catal. 190 (2000) 199–204.
[48] J.T. Miller, A.J. Kropf, Y. Zha, J.R. Regalbuto, L. Delannoy, C. Louis, E. Bus, J.A. van Bokhoven, J. Catal. 240 (2006) 222–234.
[49] P.J. Berlowitz, C.H.F. Peden, D.W. Goodman, J. Phys. Chem. 92 (1988) 5213–5221.
[50] T. Bunluesin, R.J. Gorte, G.W. Graham, Appl. Catal. B-Environ. 14 (1997) 105–115.
[51] J. Kugai, J.T. Miller, N. Guo, C. Song, J. Catal. 277 (2011) 46–53.
[52] Q. Fu, H. Saltsburg, M. Flytzani-Stephanopoulos, Science 301 (2003) 935–938.
[53] A.A. Phatak, N. Koryabkina, S. Rai, J.L. Ratts, W. Ruettinger, R.J. Farrauto, G.E. Blau, W.N. Delgass, F.H. Ribeiro, Catal. Today 123 (2007) 224–234.
[54] Y. Li, Q. Fu, M. Flytzani-Stephanopoulos, Appl. Catal. B-Environ. 27 (2000) 179–191.
[55] Y. Liu, Q. Fu, M. Flytzani-Stephanopoulos, Catal. Today 93–95 (2004) 241–246.
[56] B.C. Gates, Catalytic Chemistry, John Wiley & Sons, Inc., New York, 1992.
[57] D.M. Haaland, F.L. Williams, J. Catal. 76 (1982) 450–465.
[58] R. Burch, R.G. Buss, J. Chem. Soc. Faraday Trans. I 71 (1975) 913–921.
[59] S. Uemiya, N. Sato, H. Ando, Y. Kude, T. Matsuda, E. Kikuchi, J. Membr. Sci. 56 (1991) 303–313.
[60] F. Roa, J.D. Way, Ind. Eng. Chem. Res. 42 (2003) 5827–5835.
[61] N.A. Koryabkina, A.A. Phatak, W.F. Ruettinger, R.J. Farrauto, F.H. Ribeiro, J. Catal. 217 (2003) 233–239.